RSC Advances

Synthesis and Electrochemical Investigation of Novel Phosphite Based Layered Cathodes for Li-ion Batteries

Journal:	*RSC Advances*
Manuscript ID:	RA-ART-06-2015-012410
Article Type:	Paper
Date Submitted by the Author:	26-Jun-2015
Complete List of Authors:	Hameed, A; National University of Singapore, Chemistry Reddy, M. V.; National University of physics, Physics, Solid State ionics/adavnced batteries Lab; National University of Singapore, Materials Science & Engg. Sarkar, N; National University of Singapore, Chowdari, B.V.R; National University of Singapore, Vittal, Jagadese; National University of Singapore, Department of Chemistry

Cite this: DOI: 10.1039/x0xx00000x

Synthesis and Electrochemical Investigation of Novel Phosphite Based Layered Cathodes for Li-ion Batteries

A. Shahul Hameed,[a] M. V. Reddy,[bc] Nirjhar Sarkar,[b] B. V. R. Chowdari[b] and Jagadese J. Vittal[a]

Received ooth January 2012,
Accepted ooth January 2012

DOI: 10.1039/x0xx00000x

www.rsc.org/

Li-ion batteries (LIBs) are considered to be the best available energy storage device in the market to power electric vehicles (EVs) and stationary energy storage in grids for the efficient utilization of renewable energy sources. In this work a novel family of phosphite containing framework materials have been synthesized and investigated as cathode materials for Li-ion batteries. The oxalatophosphite frameworks, $A_2[(VO)_2(HPO_3)_2(C_2O_4)]$; A = Li, Na and K were prepared by hydrothermal treatment followed by dehydration. These cathodes possess a layered structure which can host the Li ions in the interlayer space. Electrochemical investigation of these materials using galvanostatic cycling, cyclic voltammetry and electrochemical impedance spectroscopy acknowledge the highly reversible Li intercalation at ~3.8 V. Improved capacity was observed for graphene composite compared to pristine sample.

Introduction

The successful evolution of Li-ion batteries (LIBs) in the past decades has garnered huge interest for Hybrid Electric Vehicles and Plug-in Electric Vehicles. In addition, highly efficient energy storage systems such as the LIBs are crucial for the much anticipated shift from fossil fuels to renewable energy sources such as solar and wind energy. However, large scale production and utilization of LIBs for these applications need significant progress in the technology which comprise the improvement of energy density of electrode materials, better operational safety and cost reduction. Emphasis on development of novel and cheaper cathode materials is one of the crucial step towards cost reduction as the cathode materials account for over 40 % of the total cost of LIBs.[1]

The main commercial and practical cathode materials include $LiCoO_2$,[2, 3] $LiMn_2O_4$,[4] $LiMn_{1.5}Ni_{0.5}O_4$,[5, 6] and $LiMPO_4$ (M = Fe, Mn).[7-10] Despite of having lesser capacity, the phosphate cathode $LiFePO_4$ outperform the commercial oxide cathodes owing to their low-cost, environmental friendliness and better safety features resulting from enhanced structural stability. Following the phenomenal demonstration of lithium storage in $LiFePO_4$, the quest for better cathode materials belonging to other polyanion family such as other phosphates,[11-14] silicates,[15, 16] borates,[17-19] sulphates,[20, 21] fluorophosphates[22, 23] and pyrophosphates[24, 25] have gained huge interest. In the process of finding novel and better cathode materials, unconventional electrode materials such as organic compounds,[26-29] Metal Organic Frameworks (MOFs),[30-34] etc., have also been explored recently.

In our previous study, a novel family of inorganic-organic hybrid materials termed as Metal OrganoPhosphate Open Frameworks (MOPOFs) were investigated as novel cathode materials for Li-ion batteries.[35, 36] These frameworks, $A_2[(VO)_2(HPO_4)_2(C_2O_4)]$; A = Li, Na and K has a layered structure and host the alkali metal cations in the inter-layer space which can be reversibly stored. This demonstrates good lithium storage in these materials working at potential of ~4 V with reasonably good theoretical capacities of 108-125 mAh g^{-1}. Interesting lithium storage in these MOPOF materials has motivated the development of an alternate family of hybrid cathode materials containing phosphite group. Though many phosphates, fluorophosphates and pyrophosphates have been investigated, phosphite containing materials have been rarely tested as LIB cathodes.[37] Few oxalatophosphites with interesting structure have been reported in the literature with amine cations as template.[38-44] Recently, a vanadium based oxalatophosphite framework carrying Li^+ ions has been reported.[45] The oxalatophosphite framework made of anionic layers of $[(VO)_2(HPO_3)_2(C_2O_4)]^{2-}$ host the alkali cations in the inter-layer space which can be reversibly extracted and possess two dimensional Li ion diffusion. Moreover, it has specific capacity of 135 mAh g^{-1} which is slightly higher than the corresponding oxalatophosphate due to decrease in the molecular weight.

In this work, we demonstrate the reversible lithium storage in novel phosphite based cathode materials, $A_2[(VO)_2(HPO_3)_2(C_2O_4)]$; (A = Li, Na and K). The hydrated phases, $K_2[(VO)_2(HPO_3)_2(C_2O_4)]\cdot 3H_2O$ and $Na_2[(VO)_2(HPO_3)_2(C_2O_4)]\cdot 2H_2O$ were prepared as single crystals by hydrothermal synthesis and their structures were elucidated by single crystal X-ray diffraction studies. Crystal structure of Li bearing phase, $Li_2[(VO)_2(HPO_3)_2(C_2O_4)]\cdot 6H_2O$ has been reported recently.[45] Electrochemical investigation of the anhydrous oxalatophosphites, $A_2[(VO)_2(HPO_3)_2(C_2O_4)]$; A

= Li, Na and K acknowledge the reversible Li intercalation in these materials at ~3.8 V.

Experimental section

All the chemicals and solvents used in this study are commercially available and used without further purification. V_2O_5 (Sigma Aldrich, purity 98 %), $H_2C_2O_4{\cdot}2H_2O$ (Merck, purity 99.5 %), KOH (BDH, purity 97 %), NaOH (BDH, purity 98 %), LiOH (Merck, purity 99 %) and H_3PO_3 (Alfa Aesar, purity 98 %) were used for the synthesis.

Synthesis of $K_2[(VO)_2(C_2O_4)(HPO_3)_2]$

Firstly, a potassium containing hydrated phase, $K_2[(VO)_2(C_2O_4)(HPO_3)_2]{\cdot}3H_2O$ was synthesized by a simple hydrothermal reaction. An aqueous mixture containing 1:1.4:2:10 molar ratio of V_2O_5, $H_2C_2O_4{\cdot}2H_2O$, KOH and H_3PO_3 was prepared in distilled water and stirred for 30 min to obtain a homogenous solution. It was transferred to a 23 mL Teflon-lined stainless steel autoclave with fill factor of ~40 % and sealed tightly. Heating of this mixture for 48 h at 120 °C under autogenous pressure, followed by slow cooling to room temperature yielded greenish platy single crystals of $K_2[(VO)_2(C_2O_4)(HPO_3)_2]{\cdot}3H_2O$. Yield ~80 %. TGA of the compound showed two weight loss in the range 30-180 ^oC, which corresponded to the loss of water molecules (calcd: 10.5%; found: 9.8%) while the loss of oxalate ligand occurs in the range of 300-550 ^oC (calcd: 10.9%; found: 9.7%). Elemental analysis. Anal. calcd for $C_2H_8K_2O_{15}P_2V_2$: C 4.67, H 1.57; found: C 4.74, H 1.53. A selected single crystal was utilized for structural analysis by single crystal X-ray diffraction technique. For electrochemical studies, the compound was prepared by cooling the reaction mixture in a shorter time leading to a green powder. It was washed thoroughly with deionised water, vacuum dried and dehydrated at 150 ^oC in vacuum to get the anhydrous phase, $K_2[(VO)_2(C_2O_4)(HPO_3)_2]$ for battery testing.

Synthesis of $Na_2[(VO)_2(C_2O_4)(HPO_3)_2]$

Synthesis of the precursor, $Na_2[(VO)_2(C_2O_4)(HPO_3)_2]{\cdot}2H_2O$ was carried out by a similar hydrothermal reaction at 120 °C for 48 h using a mixture of V_2O_5, $H_2C_2O_4{\cdot}2H_2O$, NaOH, H_3PO_3 and deionised water in a molar ratio of 1:1.4:6:4:500. Bluish green single crystals of the compound were obtained by slow cooling of the reaction mixture. Yield ~80 %. TGA of the compound showed two weight loss steps corresponding to the loss of 2 water molecules (calcd: 7.8%; found: 8.2%) while the loss of CO occurs in the range of 350-650 ^oC (calcd: 12.0%; found: 12.8%). Elemental analysis. Anal. calcd for $C_2H_6Na_2O_{14}P_2V_2$: C 5.18, H 1.30; found: C 5.27, H 1.29. The anhydrous phase was prepared similar to the K analogue for electrochemical studies.

Synthesis of $Li_2[(VO)_2(C_2O_4)(HPO_3)_2]$ and graphene composite

Li containing framework, $Li_2[(VO)_2(C_2O_4)(HPO_3)_2]{\cdot}6H_2O$ was synthesized from an 1:1.4:4:20:200 mixture of V_2O_5, $H_2C_2O_4{\cdot}2H_2O$, LiOH, H_3PO_3 and deionised water by a hydrothermal reaction at 120 ^oC for 48 h. This resulted in a green precipitate of the desired product. Yield ~90 %. TGA of the compound showed two weight loss steps corresponding to the loss of 4 and 2 water molecules respectively (calcd: 21.4%; found: 20.8%). The loss of oxalate ligand as CO occurs in the range of 350-630 ^oC (calcd: 11.1%; found: 10.8%). Elemental analysis. Anal. calcd for $C_2H_{14}Li_2O_{18}P_2V_2$: C 4.77, H 2.80; found: C 4.79, H 2.74. The anhydrous phase, $Li_2[(VO)_2(C_2O_4)(HPO_3)_2]$ was obtained by heating the hexahydrate phase under vacuum at 200 ^oC. The graphene composite of $Li_2[(VO)_2(C_2O_4)(HPO_3)_2]$ was prepared by addition of GO to the reaction mixture which gets reduced during the hydrothermal reaction. The amount of graphene in the composite has been found to be ~7 % from CHNS analysis.

Structural Characterization

Crystal structures of $K_2[(VO)_2(C_2O_4)(HPO_3)_2]{\cdot}3H_2O$ and $Na_2[(VO)_2(C_2O_4)(HPO_3)_2]{\cdot}2H_2O$ were determined using single crystal X-ray diffraction. Platy single-crystals of dimension 0.22 x 0.20 x 0.06 mm^3 and 0.14 x 0.10 x 0.08 mm^3 were selected for data collection for the K and Na complexes respectively, on a Bruker AXS SMART CCD diffractometer. The detailed crystallographic data of the two crystals are summarized in Table S1 and S2. Unit cell dimensions of the two crystals were obtained by least-squares refinements, and their structures were solved by direct methods. The program SMART was used for collecting frames of data, indexing reflections and determining lattice parameters and SAINT for integration of intensity of reflections and scaling. SADABS was used for empirical absorption correction and SHELXTL was used for space-group determination, structure solution and least-squares refinements on F^2.

Powder X-ray diffraction (PXRD) patterns of the powders were recorded on a Bruker D5005 diffractometer employing graphite monochromatised Cu-K_α radiation (λ = 1.54056 Å). The morphology of the samples was examined by scanning electron microscopy. SEM micrographs of the platinum coated samples were recorded on a JEOL JSM-6700F field emission scanning electron microscope (FESEM) operated at 5 kV and 10 μA. X-ray photoelectron spectra (XPS) of the materials were recorded using a VG Scientific ESCA MK II spectrometer with monochromatic Mg-Kα radiation (1253.6 eV) and the analysis of the XPS spectra was carried out using XPS Peak-fit software. Elemental analysis (EA) was carried out using a CHNS elemental analyzer (Elementar Vario MICRO CUBE). Thermogravimetric analysis (TGA) was carried out in N_2 flow with samples weighing ~10 mg at a heating rate of 5 ◦C min^{-1} using SDT 2960 TGA thermal analyzer. FT-IR spectra of the materials were recorded using KBr pellet method. Around 2 mg of each compound were ground with dry KBr powder and made into pellets and the spectra were measured in the range 4000-400 cm^{-1} on Bio-Rad FTS165 FTIR spectrophotometer.

Electrochemical Characterization

Electrochemical properties of the anhydrous oxalatophosphite cathodes were investigated using coin cells (type 2016) with Li metal (Kyokuto Metal Co., Japan) as counter electrode, glass microfiber filter (GF/F, Whatman Int. Ltd., Maidstone, England) as separator and 1 M $LiPF_6$ in ethylene carbonate (EC), dimethyl carbonate (DMC) and diethyl carbonate (DEC) (1:1:1 v/v, Merck) as the electrolyte. To fabricate the electrode films, a slurry was prepared by mixing the material with super P carbon black and PVDF binder, Kynar 2801 in a weight ratio of 70:20:10 using N-methyl pyrrolidinone (NMP) as solvent. The slurry was stirred for 12 h and then coated onto an etched aluminium foil, dried at 80 ^{o}C and punched into circular electrodes of 16 mm diameter. The coin cells were assembled in an Ar-filled glove box (MBraun, Germany) with oxygen and water concentration maintained below 1 ppm, by crimp sealing the thus fabricated electrode with lithium metal as the counter electrode. The cells were aged for 8 h before subjecting to the electrochemical testing. Galvanostatic discharge−charge cycling studies of the cells were carried out at room temperature using computer controlled Bitrode multiple battery tester (model SCN, Bitrode, U.S.A.). Electrochemical impedance spectroscopy (EIS) measurements were carried out in the frequency range of 180 kHz to 0.003 Hz using a Solartron 1260A impedance analyzer.

Results and Discussion

Structure and Morphology

Crystal structure analysis of $K_2[(VO)_2(HPO_3)_2(C_2O_4)]\cdot 3H_2O$ by single crystal X-ray diffraction reveals that it crystallizes in the monoclinic space group *C*2/*c* with following lattice parameters; a = 17.749(1) Å, b = 6.370(4) Å, c = 13.977(9) Å, β = 115.42(1)°, V = 1427.2(1) Å^3 and Z = 4. The asymmetric unit contains half the formula unit. The structure is made of infinite one dimensional $VOHPO_3$ chains along the *b*-axis (Fig. 1a) which are interlinked by oxalate ligand in bis-bidendate fashion to form infinite 2D anionic layers of $[VO(HPO_3)(C_2O_4)]^{2-}$ along the *ab*-plane (Fig. 1b). In this compound, the vanadium atoms form distorted VO_6 octahedra which are corner-shared with three different $(HPO_3)^{2-}$ units and coordinated to a terminal oxo ligand while other two coordination are to an oxalate unit. Similar coordination geometry have been reported for many oxalatophosphates and oxalatophosphites.[38-45] The anionic layers, in turn, are stacked along the *c*- direction by K^+ ions and water molecules to form a 3D structure as shown in Fig. 1c. The K^+ ions are also located in 16-membered channels formed along the *c*-axis. The V-O bond lengths are in the range of 1.987(3)-2.302(3) Å except for the vanadyl (V=O) group which has a shorter bond length of 1.589(3) Å. The P-O bond lengths in the hydrogenphosphite (HPO_3) units are 1.513(3), 1.516(3) and 1.520(3) Å. These bond lengths are well within the reported values.[38-45] Table 1 summarizes the crystallographic data and refinement details of the compound.

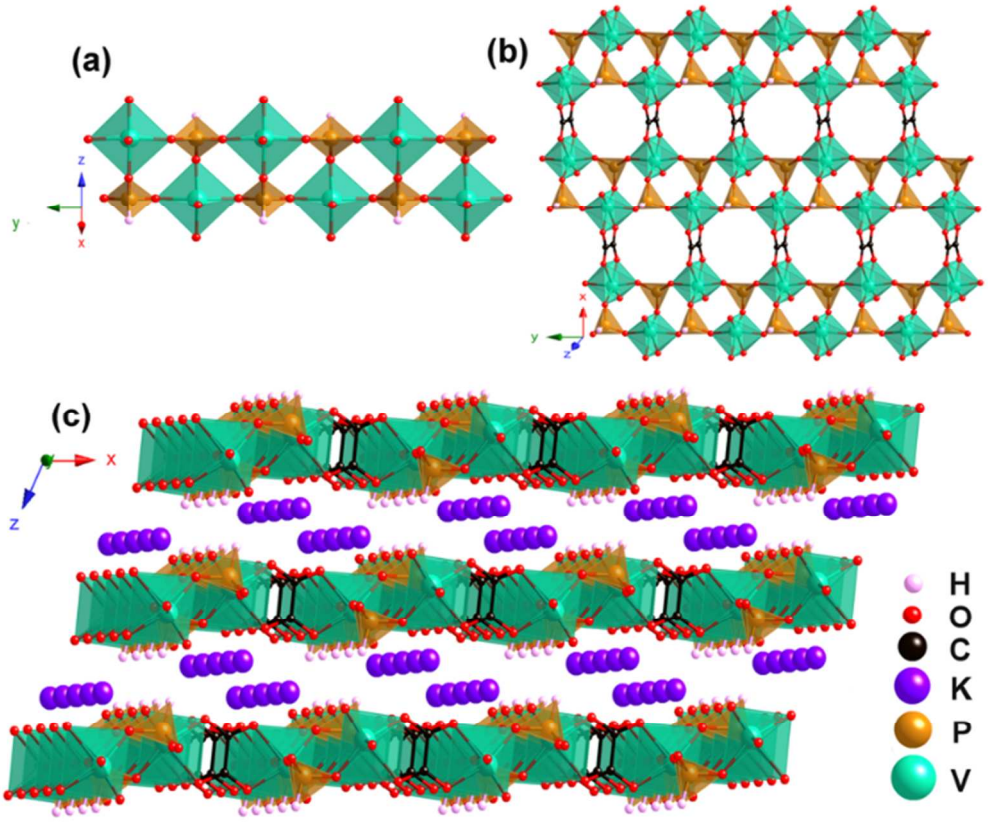

Fig. 1 Crystal structure of $K_2[(VO)_2(HPO_3)_2(C_2O_4)]\cdot 3H_2O$; (a) Perspective view of $VOHPO_3$ chains along *b*-axis; (b) Formation of $[(VO)_2(HPO_3)_2(C_2O_4)]$ layer along *ab*-plane due to interlinking of $VOHPO_3$ chains by oxalate ligand and (c) Stacking of the anionic layers along *c*-axis result in the layered structure with K^+ ions between the layers. The water molecules present in the inter-layer space are not shown for clarity.

The material $Na_2[(VO)_2(HPO_3)_2(C_2O_4)]\cdot 2H_2O$ crystallizes in the triclinic space group $P\bar{1}$. The lattice parameters are a = 6.3255(4) Å, b = 6.7760(5) Å, c = 8.0759(6) Å, α = 104.99(1)°, β = 101.67(1)°, γ = 99.12(1)°, V = 319.20(4) Å^3 and Z = 1. The structure of this framework is similar to that of K analogue. However, the $VOHPO_3$ chains that are formed along *a*-axis are linked by oxalate ligand to form anionic layers of $[(VO)_2(HPO_3)_2(C_2O_4)]^{2-}$ the $(01\bar{1})$ plane. Parallel stacking of these layers by Na^+ ions and water molecules along the *c*-axis leads to the 3D structure of $Na_2[(VO)_2(HPO_3)_2(C_2O_4)]\cdot 2H_2O$ as shown in Fig. S1. Powder X-ray diffraction (PXRD) pattern of the bulk powder matches with the simulated pattern indicating the phase purity of the sample as shown in Fig. S2. Detailed crystallographic data and refinement details of the compound are summarized in Table 1.

Table 1. Crystal data and structure refinement details of $K_2[(VO)_2(HPO_3)_2(C_2O_4)]\cdot 3H_2O$ and $Na_2[(VO)_2(HPO_3)_2(C_2O_4)]\cdot 2H_2O$

Empirical formula	**$C_2H_8K_2O_{15}P_2V_2$**	**$C_2H_6Na_2O_{14}P_2V_2$**
Formula weight	512.09	463.87
Temperature	223(2) K	223(2) K
Wavelength	0.71073 Å	0.71073 Å
Crystal system	Monoclinic	Triclinic
Space group	*C*2/*c*	$P\bar{1}$
Empirical formula	$C_2H_8K_2O_{15}P_2V_2$	$C_2H_6Na_2O_{14}P_2V_2$
Formula weight	512.09	463.87
Unit cell dimensions	*a* = 17.749(15) Å *b* = 6.370(4) Å *c* = 13.977(9) Å α = 115.421(13)°	*a* = 6.3255(4) Å *b* = 6.7760(5) Å *c* = 8.0759(6) Å α = 104.9920(10)° β = 101.6790(10)° γ = 99.1200(10)°
Volume	1427.2(18) Å^3	319.20(4) Å^3
Z	4	1
Density (calculated)	2.383 g cm^{-3}	2.413 g cm^{-3}
Absorption coefficient	2.196 mm^{-1}	1.859 mm^{-1}
F(000)	1008	228
Crystal size	0.22 x 0.20 x 0.06 mm^3	0.14 x 0.10 x 0.08 mm^3
Theta range for data collection	2.54 to 27.49°	2.70 to 27.48°
Index ranges	-22<=h<=23 -7<=k<=8 -18<=l<=18	-8<=h<=8 -8<=k<=8 -10<=l<=10
Reflections collected	4750	4133
Independent reflections	1638 [R(int) = 0.0362]	1454 [R(int) = 0.0218]
Completeness to θ = 27.49°	99.8 %	99.9 %
Absorption correction	Semi-empirical from equivalents	Semi-empirical from equivalents
Max. and min. transmission	0.8795 and 0.6437	0.8655 and 0.7808

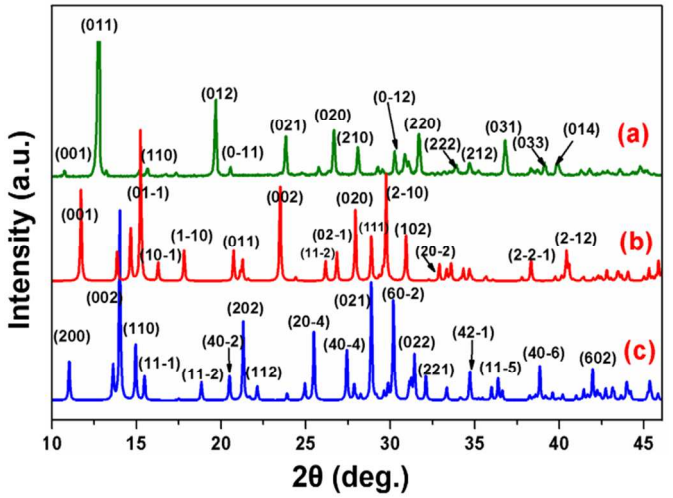

Fig. 2 PXRD patterns of (a) $Li_2[(VO)_2(HPO_3)_2(C_2O_4)]\cdot 6H_2O$; (b) $Na_2[(VO)_2(HPO_3)_2(C_2O_4)]\cdot 2H_2O$ and (c) $K_2[(VO)_2(HPO_3)_2(C_2O_4)]\cdot 3H_2O$

The lithium framework, $Li_2[(VO)_2(HPO_3)_2(C_2O_4)]\cdot 6H_2O$ was obtained as a green precipitate and its PXRD pattern (Fig. S3) matches well with the reported powder pattern of the compound. It exhibits the triclinic space group $P\bar{1}$ and the hkl fitting of the XRD pattern by TOPAS program reveals the lattice parameters to be a = 6.355(2) Å, b = 8.064(3) Å, c = 9.161(3) Å, α = 64.43(1)°, β = 87.32(2)° and γ = 67.68(3)° which are close to the reported values.[45] The PXRD patterns of the three frameworks are compared in Fig. 2.

X-ray photoelectron spectroscopy (XPS) studies of $K_2[(VO)_2(HPO_3)_2(C_2O_4)]\cdot 3H_2O$ were carried out to understand the chemical state and characteristic binding energies of the elements present (V, K, P, and O) in the framework. The binding energies of the different elements are shown separately in Fig. 3a-c. The spectrum of K2p (shown in Fig. 3a) is characterized by two peaks with binding energies of 293.10 (±0.2) and 295.94 (±0.2) eV, which correspond to the energy levels, $K2p_{3/2}$ and $K2p_{1/2}$ respectively as a result of spin orbit coupling. The peaks at 284.77(±0.2) and 288.78(±0.2) eV (Fig. 3a) are due to C1s from the oxalate ligand and the binding energies are characteristics of C-C and O-C=O groups of the oxalate ligand. The binding energy of P2p is found to be of 132.91 (±0.2) eV (Fig. 3b), characteristics of the HPO_3 group. Similar binding energy of 132.9 eV is observed for P2p level in Na_2HPO_3. The spin orbit coupling of V2p results in two peaks with binding energies of 516.90(±0.2) and 524.54(±0.2) eV, which are assigned for the $V2p_{3/2}$ and $V2p_{1/2}$ energy levels (Fig. 3c). Similar values have been reported earlier for V^{4+} system.[36] Bond valence calculations for the vanadium atoms (4.06) also confirms the oxidation state of +4 in the material.

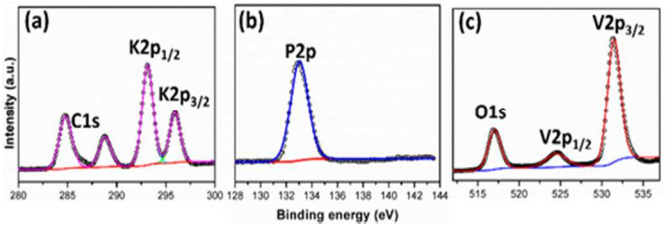

Fig. 3 XPS spectra of individual elements of $K_2[(VO)_2(HPO_3)_2(C_2O_4)]\cdot 3H_2O$; (a) K2p, C1s; (b) P2p and (c) O1s, V2p.

Morphology of the prepared framework materials was investigated using scanning electron microscopy. The SEM images of the frameworks (shown in Fig. 4a-c) indicate the formation of the compounds with plate-like morphology due to their layered structure. The particle size of the frameworks range between few hundred nm and few microns. The graphene composite is found to have particle size of few hundred nm embedded in graphene layers. However, the composite was found to be inhomogeneous as the reduction of GO to graphene happens prior to the precipitation of graphene sheets prior to the formation of the oxalatophosphite compound.

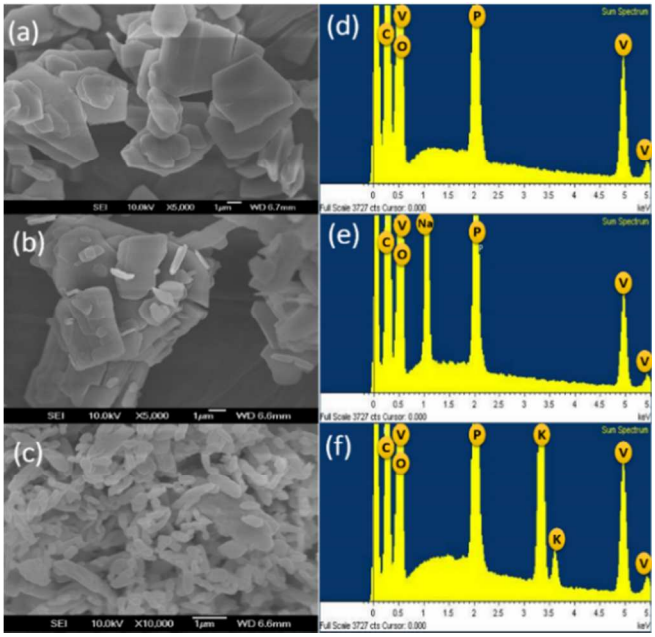

Fig. 4 SEM micrographs of (a) $Li_2[(VO)_2(HPO_3)_2(C_2O_4)]\cdot 6H_2O$, (b) $Na_2[(VO)_2(HPO_3)_2(C_2O_4)]\cdot 2H_2O$ and (c) $K_2[(VO)_2(HPO_3)_2(C_2O_4)]\cdot 3H_2O$ (scale bar: 1 µm) and (d, e & f) EDX spectra of the Li, Na and K containing frameworks respectively.

Energy dispersive X-ray (EDX) mapping of the three materials (Fig. S5-S7) show homogeneous distribution of the respective elements present in the individual samples. Fig. 4d-f show the EDX spectra of the samples, confirming the presence of V, P and alkali metal (K/Na) in ~1:1:1 ratio, which is in agreement with the proposed molecular formula. The amount of water in bulk sample were confirmed from CHNS elemental analysis and thermogravimetric analysis (TGA) shown in Fig. S8. The weight loss of ~ 20.8, 8.1 and 9.8 % correspond to the removal six, two and three moles of water from the Li, Na and K containing compounds respectively. The dehydration temperatures and the thermal stability of anhydrous frameworks were also determined from the TGA curves. The anhydrous samples were prepared from the hydrated phases by dehydration in vacuum and used for electrochemical analysis. FT-IR studies of the frameworks (Fig. S9) also support the presence of oxalate ligand from its characteristic bands at 1655 cm^{-1} and phosphite from the group of bands at ~1100-900 cm^{-1} which are identical with reported values of oxalatophosphite compounds.[43, 45]

Battery testing

Electrochemical properties of the novel cathode materials, $A_2[(VO)_2(HPO_3)_2(C_2O_4)]$; where A = Li, Na and K were investigated using coin cells by galvanostatic charge–discharge cycling studies. The experiments were carried out at room temperature with lithium metal as counter electrode in the voltage range, 2.5–4.5 V vs. Li/Li^+ at a current rate of C/10. Fig. 5a-c shows the charge-discharge profiles of the three frameworks for few selected cycles. The lithium storage in these compounds occur via V^{4+}/V^{5+} redox mechanism as evidenced by the electrochemical reaction at ~3.8 V. As can be seen from Fig. 5a, the first charge profile of $Li_2[(VO)_2(HPO_3)_2(C_2O_4)]$ exhibits a flat plateau at 4.1 V which involves the extraction of Li^+ ions from the framework resulting in the delithiated phase, $(VO)_2(HPO_3)_2(C_2O_4)$. The first charge capacity was found to be 129 mAh g^{-1} which is close to the theoretical capacity of 135 mAh g^{-1}. The first discharge reaction occurs in the material by re-intercalation of lithium ions into the framework by a single electron transfer at ~3.8 V. However, the discharge capacity was rather low, ~54 mAh g^{-1} indicating that only half of the Li^+ ions were re-intercalated. The second and subsequent cycles involve similar redox reaction in which the framework is subjected to reversible lithium insertion/extraction at 3.8 V accompanied by reduction/oxidation of vanadium in the framework. Similar plateau was observed for the oxalatophosphate material, $Li_2[(VO)_2(HPO_4)_2(C_2O_4)]$ in our previous study. However, the voltage of the redox reaction slightly decrease by 0.1 V from ~3.9 to 3.8 V because of replacement of HPO_4 by HPO_3 unit as the phosphate group has stronger inducting effect. With increase in the cycle number, the lithium storage improves slightly and a discharge capacity 64 mAh g^{-1} was observed at the end of 40 cycles (Fig. 4 d). The slight increase in the capacity of the framework may be explained by the decrease in the particle size upon cycling, often termed as 'electrochemical grinding effect'. The coulombic efficiency of the 1st cycle is low but improves in the subsequent cycles. The redox reaction responsible for the reversible lithium storage in this material is shown below.

$$Li_2[(VO)_2(HPO_3)_2(C_2O_4)] \leftrightarrow [(VO)_2(HPO_3)_2(C_2O_4)] + 2Li^+ + 2e^-$$

The initial charge cycle of the Na containing framework, $Na_2[(VO)_2(HPO_3)_2(C_2O_4)]$ involves the removal of Na^+ ions

from the layered structure resulting in the bare framework and the corresponding oxidation of V^{4+} to V^{5+} at ~4.1 V (Fig. 5b). During the first discharge cycle, Li^+ ions are preferably re-inserted into the framework than the Na^+ ions. This preferable lithium insertion has been demonstrated in earlier reports.[36] Upon further cycling, Li^+ ions are reversibly extracted from the framework, forming the lithiated and delithiated frameworks upon discharge and charge reactions respectively at ~3.8 V. At the end of 40 cycles, $Na_2[(VO)_2(HPO_3)_2(C_2O_4)]$ exhibits a discharge capacity of 54 mAh g^{-1}. The coulombic efficiency which was 76% for the 1st cycle increased to 91% for the 40th cycle.

The potassium containing cathode, $K_2[(VO)_2(HPO_3)_2(C_2O_4)]$ exhibits a different electrochemical behavior compared to other two phases. The first charge cycle shows two plateaus at ~3.9 V and 4.3 V (Fig. 4c) which can be explained as the removal of K^+ ions in two steps with the formation of $K[(VO)_2(HPO_3)_2(C_2O_4)]$ phase in between. Similar extraction of Li^+ ion in two steps is observed in another cathode material, $Li_3V_2(PO_4)_3$.[14] The first discharge curve also shows two plateaus at 3.8 and 3.6 V indicating the Li re-insertion into the framework occurs in two steps. After few cycles, the second plateau disappears and the lithium storage arises only from a single sloping plateau at 3.8 V as seen in Fig. 5c. The charge and discharge capacity of the material at the end of 40 cycles were 59 and 56 mAh g^{-1} respectively.

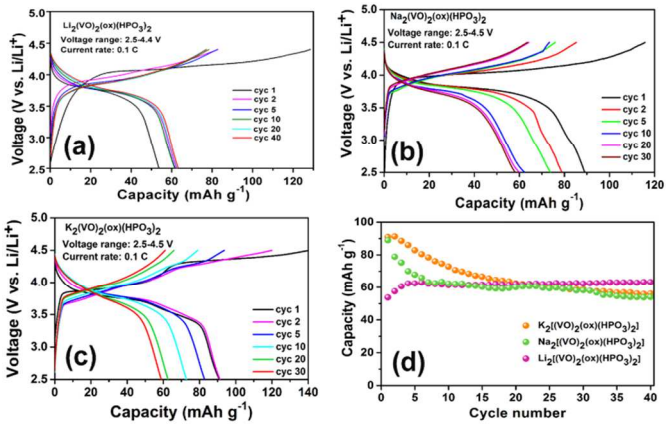

Fig. 5 Galvanostatic cycling studies showing charge-discharge profiles in the voltage window, 2.5-4.5 V (a) $Li_2[(VO)_2(HPO_3)_2(C_2O_4)]$ at 0.1 C current rate (13.5 mA g^{-1}); (b) $Na_2[(VO)_2(HPO_3)_2(C_2O_4)]$ at 0.1 C current rate (12.5 mA g^{-1}); (c) $K_2[(VO)_2(HPO_3)_2(C_2O_4)]$ at 0.1 C current rate (12 mA g^{-1}) and (d) Variation of capacity (discharge) with cycle number of the different oxalatophosphite materials.

As the lithiated sample shows the best performance among the three cathodes, its graphene composite was prepared to improve the lithium storage. Addition of GO in the reaction mixture during the hydrothermal reaction yielded the composite material. As shown in Fig. 6, the capacity of the composite was better than the pristine sample due to increase in the conductivity. However, the composite was inhomogeneous and the interaction between graphene and $Li_2[(VO)_2(HPO_3)_2(C_2O_4)]$ was weak. This leads to slight capacity fading after ~20 cycles. The coulombic efficiency also improved from 80 % to 96% for the graphene composite. Improvement can be anticipated by preparation of homogeneous nanocomposite. Further careful studies during charge-discharge cycling by in-situ X-ray and neutron diffraction studies and other complementary spectroscopy and microscopy techniques are needed to explain detail reaction mechanism.

Cyclic voltammetry (CV) is a complementary technique to galvanostatic cycling which gives information about the redox potentials of electrochemical reactions occurring in the electrodes. CV curves of the materials for the first cycle at a scan rate of 0.058 mV s^{-1} are shown in Fig. 7a. As observed in the galvanostatic cycling, the charge and discharge of $K_2[(VO)_2(HPO_3)_2(C_2O_4)]$ is characterized by two redox couples. Anodic scan (oxidation) of the sample shows two overlapping peaks at ~3.95 and 4.25 V while the cathodic scan has two close peaks at 3.7 and 3.5 V. In contrary, the lithium framework has only one redox couple at 4.25 and 3.5 for the anodic and cathodic scans which agrees with the galvanostatic cycling results. Similar voltages were observed for the V^{4+}/V^{5+} redox couple in oxalatophosphate cathodes.[36,37]

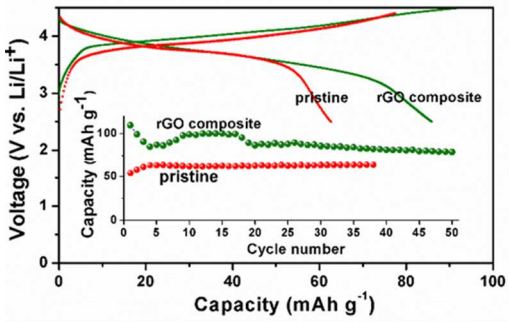

Fig. 6 Comparison of charge-discharge profiles of pristine sample and rGO composite of $Li_2[(VO)_2(HPO_3)_2(C_2O_4)]$ with the inset figure showing their discharge capacity vs. cycle number.

ElS is an electroanalytical technique used to analyse electrode kinetics. The impedance measurements were carried out for $Li_2[(VO)_2(HPO_3)_2(C_2O_4)]$ during charge and discharge at selected voltages. During each voltage increment (charging) and decrement (discharging), the cell was subjected to a current density of ~30 mA g^{-1} and was relaxed at the given voltage for 2 h before data collection. The results are plotted as Nyquist plots (Z_{re} vs. Z_{im}), where Z_{re} and Z_{im} are respectively the real and imaginary parts of cell impedance. Fig. 7b shows the Nyquist plots of the material. At OCV of ~2.9 V, a single semicircle with an overall impedance of ~175 Ω was observed which is attributed to the surface film resistance and charge transfer resistance (R_{sf} + R_{ct}) and the associated capacitances (CPE_{sf} and CPE_{dl}) despite a single semicircle was observed. With the onset of lithium extraction from the electrode, surface film ruptures and a decrease in impedance to ~130 Ω was noticed at the charge plateau (3.8-4.0 V). At the fully charged state, vanadium becomes insulating (V^{5+}) and as a result, a high impedance of 440 Ω was observed. However, upon discharge the impedance decreases to 160 Ω where the Li insertion takes

place. The difference in the charge and discharge capacities of the samples can be interpreted as the higher impedance during the discharge compared to the charge cycle.

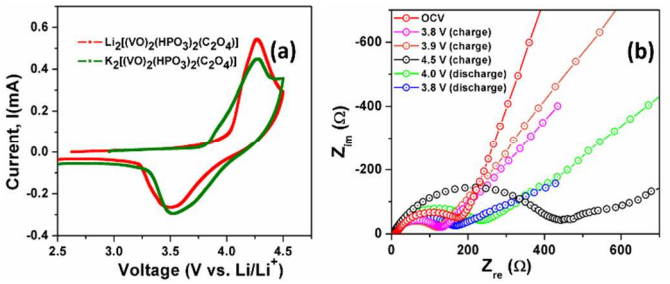

Fig. 7 (a) CVs of $Li_2[(VO)_2(HPO_3)_2(C_2O_4)]$ and $K_2[(VO)_2(HPO_3)_2(C_2O_4)]$ and (b) Nyquist plots of $Li_2[(VO)_2(HPO_3)_2(C_2O_4)]$ at different voltages.

Conclusions

In summary, we have demonstrated the reversible lithium storage in a novel family of phosphite containing hybrid cathode materials for Li-ion battery application. The facile migration pathways in the layered structure highlight the material's property and the high voltage of 3.8 V assists in achieving good energy density. Electrochemical investigation of the frameworks manifest the reversible extraction of alkali metal ions and re-insertion of Li ions into the layered structure. This flexibility of having different alkali metal cation in the prepared framework helps in choosing the best and cheapest material among them which can decrease the overall cost of electrode materials. In the current study, though the materials were shown to have good reversible lithium storage, the capacity was slightly poor due to its conductivity and bigger particle size of the compounds. Attempts to prepare graphene composite of $Li_2[(VO)_2(HPO_3)_2(C_2O_4)]$ resulted in an improved performance due to increased conductivity. Nevertheless, further structural studies on cycled electrodes during cycling by in-situ X-ray, neutron diffraction and other spectroscopy techniques are needed to understand electrochemical mechanisms of these materials. With low synthetic temperature, good theoretical capacity of 135 mAh g^{-1} and high voltage of 3.8 V, $Li_2[(VO)_2(HPO_3)_2(C_2O_4)]$ can create interest for new directions in the research for novel cathode materials.

Acknowledgements

The authors thank Ms Geok Kheng Tan and Ms Hong Yimian for the collection of X-ray crystallographic data

Notes

‡ CCDC 1040912 and 1040913 contains the supplementary crystallographic data for this paper. These data can be obtained free of charge from The Cambridge Crystallographic Data Centre via www.ccdc.cam.ac.uk/data_request/cif

[a]Department of Chemistry, National University of Singapore, Singapore 117543. Fax: (+) 65-6779-1691; E-mail: chmjjv@nus.edu.sg

[b]Advanced batteries lab, Department of Physics, National University of Singapore, Singapore 117542. Fax: (+) 65-6777-6126; E-mail: phymvvr@nus.edu.sg

[c]Department of Materials Science and Engineering, National University of Singapore, Singapore

References

1. R. J. Brodd and C. Helou, *J. Power Sources*, 2013, 231, 293-300.
2. K. Tan, M. Reddy, G. Rao and B. Chowdari, *J. Power Sources*, 2005, 147, 241-248.
3. M. Jo, M. Noh, P. Oh, Y. Kim and J. Cho, *Adv. Energy Mater.*, 2014, 4, 1301583.
4. Y. Xia and M. Yoshio, *J. Electrochem. Soc.*, 1996, 143, 825-833.
5. M. V. Reddy, H. Y. Cheng, J. H. Tham, C. Y. Yuan, H. L. Goh and B. V. R. Chowdari, *Electrochim. Acta*, 2012, 62, 269-275.
6. C. J. Jafta, M. K. Mathe, N. Manyala, W. D. Roos and K. I. Ozoemena, *ACS Appl. Mater. Interfaces*, 2013, 5, 7592-7598.
7. J. Liu, M. N. Banis, Q. Sun, A. Lushington, R. Li, T.-K. Sham and X. Sun, *Adv. Mater.*, 2014, 26, 6358.
8. A. K. Padhi, K. S. Nanjundaswamy and J. B. Goodenough, *J. Electrochem. Soc.*, 1997, 144, 1188-1194.
9. S.-Y. Chung, J. T. Bloking and Y.-M. Chiang, *Nat. Mater.*, 2002, 1, 123-128.
10. V. Aravindan, J. Gnanaraj, Y.-S. Lee and S. Madhavi, *J. Mater. Chem. A*, 2013, 1, 3518-3539.
11. H. Huang, S.-C. Yin, T. Kerr, N. Taylor and L. F. Nazar, *Adv. Mater.*, 2002, 14, 1525-1528.
12. H. Karami and F. Taala, *J. Power Sources*, 2011, 196, 6400-6411.
13. A. S. Hameed, M. Nagarathinam, M. Reddy, B. Chowdari and J. J. Vittal, *J. Mater. Chem.*, 2012, 22, 7206-7213.
14. A. S. Hameed, M. Reddy, B. Chowdari and J. J. Vittal, *Electrochim. Acta*, 2014, 128, 184-191.
15. S. J. Kim, J. Suk, Y. J. Yun, H.-K. Jung and S. Choi, *Phys. Chem. Chem. Phys.*, 2014, 16, 2085-2089.
16. T. Muraliganth, K. R. Stroukoff and A. Manthiram, *Chem. Mater.*, 2010, 22, 5754-5761.
17. A. Yamada, N. Iwane, Y. Harada, S.-i. Nishimura, Y. Koyama and I. Tanaka, *Adv. Mater.*, 2010, 22, 3583-3587.
18. L. Tao, G. Rousse, J. N. Chotard, L. Dupont, S. Bruyere, D. Hanzel, G. Mali, R. Dominko, S. Levasseur and C. Masquelier, *J. Mater. Chem. A*, 2014, 2, 2060-2070.
19. Y. Janssen, D. S. Middlemiss, S.-H. Bo, C. P. Grey and P. G. Khalifah, *J. Am. Chem. Soc.*, 2012, 134, 12516-12527.
20. P. Barpanda, M. Ati, B. C. Melot, G. Rousse, J. N. Chotard, M. L. Doublet, M. T. Sougrati, S. A. Corr, J. C. Jumas and J. M. Tarascon, *Nat. Mater.*, 2011, 10, 772-779.
21. J. M. Clark, C. Eames, M. Reynaud, G. Rousse, J.-N. Chotard, J.-M. Tarascon and M. S. Islam, *J. Mater. Chem. A*, 2014, 2, 7446-7453.
22. J. Barker, M. Y. Saidi and J. L. Swoyer, *J. Electrochem. Soc.*, 2003, 150, A1394-A1398.
23. M. V. Reddy, G. V. Subba Rao and B. V. R. Chowdari, *J. Power Sources*, 2010, 195, 5768-5774.
24. M. Tamaru, P. Barpanda, Y. Yamada, S.-i. Nishimura and A. Yamada, *J. Mater. Chem.*, 2012, 22, 24526-24529.
25. S.-i. Nishimura, M. Nakamura, R. Natsui and A. Yamada, *J. Am. Chem. Soc.*, 2010, 132, 13596-13597.
26. Z. Zhu, M. Hong, D. Guo, J. Shi, Z. Tao and J. Chen, *J. Am. Chem. Soc.*, 2014, 136, 16461-16464.
27. Y. Hanyu, Y. Ganbe and I. Honma, *J. Power Sources*, 2013, 221, 186-190.
28. Y. Hanyu and I. Honma, *Sci. Rep.*, 2012, 2, 453.
29. Y. Hanyu, T. Sugimoto, Y. Ganbe, A. Masuda and I. Honma, *J. Electrochem. Soc.*, 2014, 161, A6-A9.
30. S.-L. Li and Q. Xu, *Energy Environ. Sci.*, 2013, 6, 1656-1683.
31. X. Li, F. Cheng, S. Zhang and J. Chen, *J. Power Sources*, 2006, 160, 542-547.
32. J. Xiang, C. Chang, M. Li, S. Wu, L. Yuan and J. Sun, *Cryst. Growth Des.*, 2007, 8, 280-282.
33. G. Férey, F. Millange, M. Morcrette, C. Serre, M.-L. Doublet, J.-M. Grenèche and J.-M. Tarascon, *Angew. Chem. Int. Ed.*, 2007, 46, 3259-3263.

34. G. de Combarieu, M. Morcrette, F. Millange, N. Guillou, J. Cabana, C. P. Grey, I. Margiolaki, G. Ferey and J. M. Tarascon, *Chem. Mater.*, 2009, 21, 1602-1611.
35. A. Shahul Hameed, M. Nagarathinam, M. Schreyer, M. V. Reddy, B. V. R. Chowdari and J. J. Vittal, *J. Mater. Chem. A*, 2013, 1, 5721-5726.
36. M. Nagarathinam, K. Saravanan, E. J. H. Phua, M. V. Reddy, B. V. R. Chowdari and J. J. Vittal, *Angew. Chem. Int. Ed.*, 2012, 51, 5866-5870.
37. H. Y. Asl, K. Ghosh, M. P. Vidal Meza and A. Choudhury, *J. Mater. Chem. A*, 2015, 3, 7488-7497.
38. C. Li, L. Huang, M. Zhou, J. Xia, H. Ma, S. Zang and L. Wang, *J. Solid State Chem.*, 2013, 208, 86-92.
39. H. Li, L. Zhang, Q. Huo and Y. Liu, *J. Solid State Chem.*, 2013, 197, 75-80.
40. H. Li, L. Zhang, L. Liu, T. Jiang, Y. Yu, G. Li, Q. Huo and Y. Liu, *Inorg. Chem. Commun.*, 2009, 12, 1020-1023.
41. Z. Lin, H. P. Nayek and S. Dehnen, *Microporous Mesoporous Mater.*, 2009, 126, 95-100.
42. L. Liu, D. Luo, D. Li and Z. Lin, *Dalton Trans.*, 2014, 43, 7695-7698.
43. S. Mandal and S. Natarajan, *Chem. - Eur. J.*, 2007, 13, 968-977.
44. P. Ramaswamy, N. N. Hegde, R. Prabhu, V. M. Vidya, A. Datta and S. Natarajan, *Inorg. Chem.*, 2009, 48, 11697-11711.
45. S. Auguste, V. Alonzo, T. Bataille, L. Le Polles, W. Canon-Mancisidor, D. Venegas-Yazigi and E. Le Fur, *J. Solid State Chem.*, 2014, 211, 212-218.

TOC Graphic

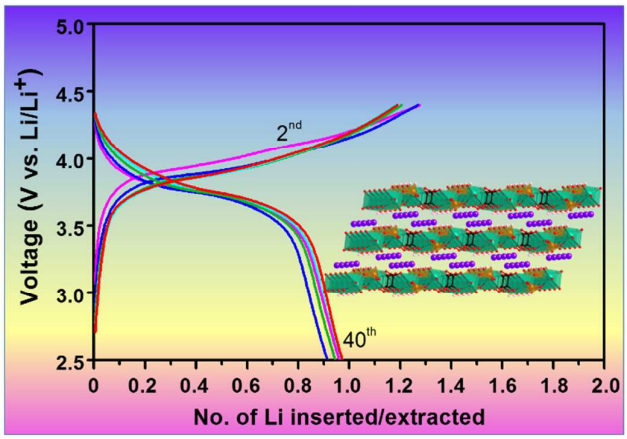

Reversible lithium storage has been demonstrated in novel phosphite containing cathode materials, $A_2[(VO)_2(HPO_3)_2(C_2O_4)]$; A=Li, Na and K.